Ionization distances of Rydberg atoms approaching solid surfaces in the presence of weak electric fields

N. N. Nedeljković and Lj. D. Nedeljković*
Faculty of Physics, University of Belgrade, P.O. Box 368, Belgrade, Serbia and Montenegro, Yugoslavia
(Received 27 April 2005; published 30 September 2005)

The ionization distances R_c^I of slow hydrogenlike Rydberg atoms approaching solid surfaces in the presence of a weak external electric field are calculated. The ionization is treated as resonant electron tunneling in the very vicinity of the top of the potential barrier, created between the ionic core and polarized solid. We obtain both the complex energies and the ionization distances by solving the energy eigenvalue problem under the outgoing wave boundary condition towards the solid. The eigenvalue problem is studied in parabolic coordinates within the framework of an etalon equation method adapted to include the confluence of turning points. It is demonstrated that in a critical region $R \approx R_c^I \gg 1$ a.u. of ion-surface distances R, parabolic quantum numbers n_1, n_2, and m can serve as approximate, but "sufficiently good" quantum numbers, at least for lower n_1 values. The method offers asymptotically exact analytical expressions for the ionization rates and energies, which follow the theoretical predictions of the complex scaling method (CSM). It is also found that the resulting ionization distances R_c^I are in very good agreement with the results of CSM. The implications of using obtained results in analyzing the recent xenon experimental data for R_c^I are briefly discussed.

DOI: 10.1103/PhysRevA.72.032901 PACS number(s): 34.50.Dy, 79.20.Rf

I. INTRODUCTION

Recently, an interest for the relatively old and difficult problem concerning "direct observation" of ionization distances of Rydberg atoms approaching to solid surfaces was renewed [1]. In the cited experiment [1] the ionization distances R_c^I are obtained for xenon Rydberg atoms approaching a solid surface (under near grazing geometry conditions) with hyperthermal velocities ($v \ll 1$ a.u.), in the presence of a weak external electric field. The distances R_c^I are established by measuring threshold values of the electric field, which are sufficient to stop the ionized particle and send it back into a detector.

Despite the extensive theoretical study of the ionization process, the information concerning the ionization distances for Rydberg atoms remains incomplete, even for the simplest hydrogenic-type ones. The commonly used theoretical methods are very heterogenous in nature; here we mention the classical over-barrier method [2,3], the perturbation method [4], the coupled angular mode method (CAM) [5,6], the complex scaling method (CSM) [7–9], the stabilization method [10,11], the time-dependent close-coupling technique [12,13], and the two-state vector model [14–17]. Generally, two different definitions of the ionization distance have been used. The classical electron transition model [3] defines the ionization distance as the critical distance R_c at which the energy term "touches" the saddle point of the potential barrier. A more exact definition of the ionization distance R_c^I is given by quantum models. Namely, particular Rydberg states ionize over a narrow range of ion-surface distances R around $R=R_c^I$, where R_c^I is the position of maximum of total ionization rate [15,16,18]. Although these definitions have very different physical connotations, it is reasonable to expect that $R_c^I \approx R_c$ for highly excited Rydberg atoms.

The nonperturbative complex scaling method [19] was used as the basis for the first calculations of ionization distance R_c^I, devoted directly to the hydrogenic Rydberg atom approaching solid surface in the presence of external electric field. This method [7–9,19] consists of solving the eigenvalue problem of an effective non-Hermitian Hamiltonian $\hat{H}(\theta)$ of the active electron, obtained by the "complex rotation" $r \rightarrow r\exp(i\theta)$ of the electronic radial coordinate r in the Hamiltonian $\hat{H}$. Simultaneously, a diverging boundary condition of Siegert's type is transformed into the "bound-state boundary condition" (providing that the parameter θ exceeds a critical value). The diagonalization of the Hamiltonian $\hat{H}(\theta)$ gives numerical values for complex eigenenergies, and the imaginary parts of these eigenenergies correspond to the ionization rates (energy widths). The ionization distances R_c^I are derived from the total ionization rates (ionization probabilities per unit time), calculated with the obtained widths. Strongly "hybridized" eigenstates of $\hat{H}(\theta)$ have been expressed as a superposition of a large but finite number of hydrogenic bound states. An incomplete classification of these eigenstates and corresponding eigenenergies has been performed in terms of two good quantum numbers, n and m.

Although the predictions of the hydrogenic CSM model mainly reflect the experimental data [1], we realized that a few physically relevant questions have remained open within the framework of that model. First of all, the character of electron tunneling requires an additional analysis, i.e., a criterion concerning the relation of the energy-level position and the potential barrier top is worthwhile. Besides, it is not clear whether a complete classification of the electronic eigenstates is possible, at least approximately. Also, it is important to investigate whether the forms of near-surface potentials (significant at "physisorption distances" $R \sim 10$ a.u. and lower n values [8]) could play a decisive role at very large ion surface distances, e.g., $R \sim 1000$ a.u. Finally, since

*Electronic address: hekata@ff.bg.ac.yu

the highly excited Rydberg atoms manifest in part some properties of quasiclassical objects, it would be informative to test explicitly how the distances R_c and R_c^I are related.

In the present paper we discuss the problem of ionization distances R_c^I of hydrogenlike Rydberg atoms outside the complex scaling method. An appropriate nonperturbative etalon equation method [20,21] will be developed. This asymptotic method has previously been applied to a wide class of physical problems with large parameters. It enables us to point out in a more direct manner that the ionization of hydrogenlike Rydberg atoms represents a tunneling process at large ion-surface distances, $R \approx R_c \gg 1$ a.u. Our starting idea is that the resonant tunneling takes place in the very vicinity of the potential barrier top, created between the ionic core (with core charge Z) and the polarized solid, in the presence of a weak electric field F. The electron tunneling dynamics is described by a Gamow-type decaying state Ψ, representing an eigenfunction of the "nonrotated" Hamiltonian $\hat{H}$ and satisfying the surface oriented outgoing wave boundary condition. Under these conditions, the decaying eigenstate Ψ corresponds with the complex eigenenergy with an imaginary part proportional to the ionization rate.

A specific feature of the etalon equation method of solving the eigenvalue problem of $\hat{H}$ is that it does not use the decaying state Ψ as an expansion with respect to any basis of wave functions. Accordingly, the complex eigenenergies are not related with a diagonalization procedure resulting in the appearance of matrix elements of $\hat{H}$. Unlike the volume integrals over the whole space, expressing these matrix elements, the etalon equation method is based on the calculation of corresponding "etalon-method integrals" along the tunneling direction. For $R \approx R_c \gg 1$ a.u., the tunneling and atomic regions give the dominant contributions to these integrals, so that the details of the near-surface potential are avoided; see, for example, Eq. (3.6b) and the subsequent discussion in Sec. III B concerning Eqs. (3.11a) and (3.11b).

Under these circumstances, a few physically plausible approximations are possible. Namely, in the critical region $R \approx R_c$, the complex energy eigenvalue problem of $\hat{H}$ is practically separable in parabolic coordinates ξ, η, φ, at least in the most relevant region ($\xi \ll \eta$) of the electron transitions. In other words, the parabolic quantum numbers can be taken as approximate, but sufficiently good quantum numbers for a classification of the decaying eigenstates Ψ. The potentials of the electron interaction with the pointlike atomic core U_A and the external electric field F do not violate the parabolic symmetry of the Hamiltonian $\hat{H}$. Also, in the tunneling region and for $R \approx R_c \gg 1$ a.u., the classical image force potentials fit both the "true" nonsingular electron self-image potential U_M and the atomic core image potential U_{AM}. So, the physically relevant terms which approximately maintain the parabolic symmetry can be extracted from the total potential U of the Hamiltonian $\hat{H}=\hat{T}+\hat{U}$.

In solving the one-dimensional effective eigenvalue problems along the ξ and η directions, the original second-order differential equations are associated with a set of additional "etalon equations," whose solutions are well known and which have the same type of transition points (turning points and simple poles) as the original ones. In the present paper we consider the close turning point configuration, which characterizes the electron tunneling in the vicinity of the potential barrier top. Therefore, in order to obtain accurate asymptotic expressions for ionization distances, we adapt the etalon equation method to include the confluence of the turning points (in the η direction). It allows us to introduce the function $\epsilon(R)$, which represents both a spectral parameter of the corresponding etalon equation and a measure of its turning point distance. The function $\epsilon(R)$ contains the main information about critical distances R_c and ionization distances R_c^I. Namely, we will show that $\mathrm{Re}\,\epsilon(R_c)=0$ and $\mathrm{Re}\,\epsilon(R_c^I) \approx \epsilon_0$, where ϵ_0 is a given constant determined by the parameters of the system (parabolic quantum numbers, core charge, normal component of the ionic velocity, and electric field).

This paper is organized as follows. After the formulation of the problem (Sec. II), we will derive the ionization rates, energy terms, and, simultaneously, the ionization distances R_c^I (Sec. III). In Sec. IV we present the results of our calculations for typical values of parabolic quantum numbers and external electric fields. The results are compared with the predictions of CSM [9,18,19,22] and the available experimental data [1]. Some concluding remarks will be given in Sec. V. Atomic units ($e^2=\hbar=m_e=1$) will be used throughout the paper.

II. FORMULATION OF THE PROBLEM

A. Ion-surface potential in the critical region $R \approx R_c$

We consider the slow hydrogenlike Rydberg atom (core charge Z), approaching a solid surface in the presence of a weak external electric field F, directed from the solid to the vacuum (Fig. 1). We restrict ourselves to the critical region $R \approx R_c \gg 1$ of the ion-surface distances R, i.e., our attention is focused on the electron tunneling in the very vicinity of the potential barrier top. The relevant z component of the atomic core motion is described by the classical law $dR/dt=-v_\perp$, where $v_\perp$ is the corresponding component of the core velocity v.

In the low velocity region ($v_\perp \ll 1$), the adiabatic wave function Ψ behaves as a decaying state. The function Ψ is determined by the the complex energy eigenvalue problem $\hat{H}\Psi=E\Psi$ with the outgoing wave boundary condition (towards the solid) [16]. Namely, under the influence of the field of the polarized solid, the initially discrete electron state (the electron is bound to the atom) becomes quasistationary in nature, due to the possibility of electron tunneling towards the solid.

In the coordinate system located at the solid surface, with the z axis perpendicular to the surface, and in the region outside the solid ($z>0$), the Hamiltonian $\hat{H}$ of the system is given by

$$\hat{H} = -\frac{1}{2}\nabla^2 + U_A + Fz + U_M + U_{AM}. \tag{2.1}$$

For U_A we take the Coulomb potential $U_A=-Z/r_A$, where r_A is the electron position with respect to the ionic core. The

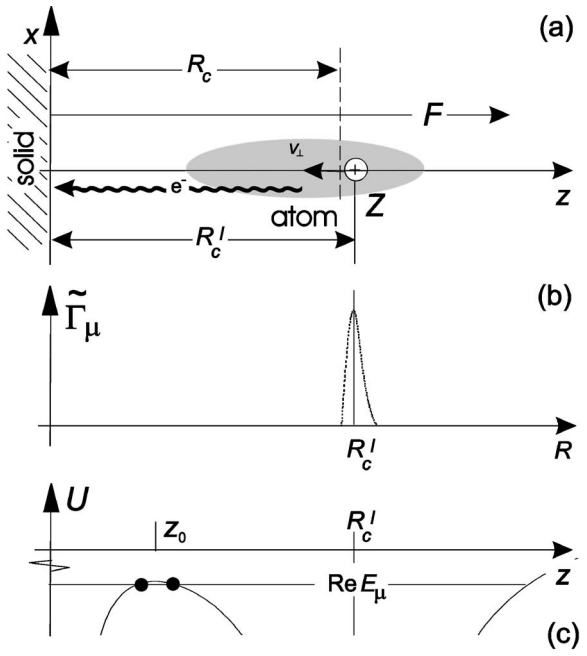

FIG. 1. (a) A schematic presentation of the ionization process in the critical region, $R \approx R_c \approx R_c^I \gg 1$. The quantity R_c is defined in the text, Eq. (2.9). (b) The total ionization rate $\tilde{\Gamma}_\mu$ determining the ionization distance R_c^I. (c) The potential U along the z axis for $R = R_c^I$ and the corresponding position of the electronic energy level Re E_μ.

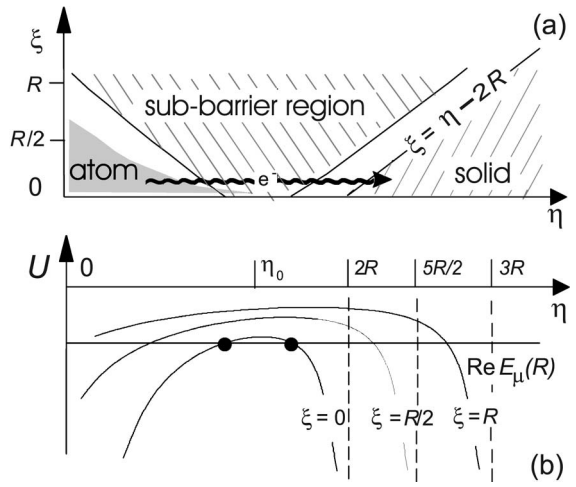

FIG. 2. (a) Relevant regions for electron transitions in the ξ, η plane. The positions of the ionic core and solid surface are given by $\xi = \eta = 0$ and $\xi = \eta - 2R$, respectively. (b) Potential barrier $U(\xi, \eta; R, Z, F)$ for $R \approx R_c \gg 1$ a.u. and $Z = 1$ along the η axis for $\xi = 0$, $\xi = R/2$, and $\xi = R$. The energy Re $E_\mu(R)$ and the corresponding turning points (dots) are also presented in (b). The Fermi level of the solid is far below the Re $E_\mu(R)$ level.

term $U_M + U_{AM}$ is the surface potential of the polarized solid.

So far, a number of "true" nonsingular (at $z = 0$) surface potentials, approaching the bulk value for $z \to 0$, have been proposed (see, for example, Refs. [3,6,8,12], and references therein). However, bearing in mind that the etalon equation method is based on the calculation of the integrals over the interval sufficiently far from the surface (see the Introduction), our model is almost independent from the concrete form of the near-surface potential. Also, for low velocities of the ionic projectile, a dynamical response of the surface can be neglected. For these reasons it is sufficiently accurate to use the classical electrostatic image approximations: the electron image potential $U_M = -1/4z$ and the potential of ionic core image $U_{AM} = Z/\sqrt{\rho^2 + (z+R)^2}$, where $\rho^2 = x^2 + y^2$. Besides, under the conditions $R \approx R_c \gg 1$, the potential inside the solid does not play a decisive role. Namely, for the tunneling in the vicinity of the potential barrier top, Fig. 1, the Fermi level and the corresponding depth U_0 of the solid potential wall are far below the instant position of the electronic level.

The first three terms in the Hamiltonian $\hat{H}$ (hydrogenlike atom in the electric field) enable the separation of variables in the parabolic coordinates $\xi = r_A + z_A$, $\eta = r_A - z_A$ and $\varphi = \arctan(y/x)$, defined in the coordinate system located at the ionic core. The term $U_M + U_{AM}$ breaks the parabolic symmetry. However, for $R \approx R_c \gg 1$ this symmetry is satisfied approximately. Namely, the potential $U = U_A + Fz + U_M + U_{AM} \equiv U(\xi, \eta; R, Z, F)$ along the η axis forms the barrier, which is shifted upwards (with broadening) with the increasing of ξ; see Fig. 2. Accordingly, the "transparency" of the barrier decreases rapidly with the increasing of ξ. Taking into account that the potential U along the ξ axis corresponds to the finite electronic motion, we conclude that the η axis is the tunneling direction, i.e., the condition $\xi \ll \eta$ for the tunneling process in the critical region is satisfied.

With this condition, in the range $\eta \in [0, \eta_0 \approx 2(R - z_0) \approx 4R/3]$, see Figs. 1(c) and 2(b), relevant for the "etalon-method integrals," we have

$$U_M + U_{AM} = \left(-\frac{1}{4\left(R - \frac{\eta}{2}\right)} + \frac{Z}{2R - \frac{\eta}{2}} \right) \left[1 + O\left(\frac{\xi}{R}\right) \right]. \tag{2.2a}$$

The approximation given by Eq. (2.2a) enables the separation of variables in the parabolic coordinates, i.e., the violation of the parabolic symmetry is localized within the term $O(\xi/R)$. Note that in the far asymptotic (deep sub-barrier) region $(R \gg R_c \gg 1)$ we have

$$U_M + U_{AM} \approx \frac{2Z-1}{4R} - \frac{Z-1}{8R^2}(\xi - \eta), \tag{2.2b}$$

so that the corresponding eigenvalue problem reduces to the Stark-like one. For the higher-order terms in the expansion (2.2b) over z_A/R and ρ/R see, for example, Ref. [6].

The complex eigenenergies of $\hat{H}$, with the parabolic symmetry approximately conserved, are labeled by the parabolic index set $\mu = (n_1, n_2, m)$ of the approximately good quantum numbers [16], i.e., we have

$$E_\mu = \text{Re}\, E_\mu - \frac{i}{2}\Gamma_\mu, \tag{2.3}$$

where Γ_μ is the corresponding ionization rate.

B. Separation of variables for $R \approx R_c$

In the separation of variables procedure, concerning the complex energy eigenvalue problem of $\hat{H}$ for $R \approx R_c$, we use the scaled parabolic coordinates $\tilde{\xi}=\xi/2R\alpha$ and $\tilde{\eta}=\eta/2R\alpha$. The scaling parameter α is defined by $\alpha=-2\tilde{E}_\mu R/(Z-1/4)$, where $\tilde{E}_\mu=E_\mu(R)-FR$. For convenience, instead of $\tilde{\eta}$ we introduce the variable $u=\sqrt{\tilde{\eta}}$ to represent the effective electron coordinate. We take the quantity $b=\sqrt{-2\tilde{E}_\mu}(2R\alpha)$ as a large parameter of the eigenvalue problem.

By omitting the small term $O(\xi/R)$ in Eq. (2.2a), and taking that $\Psi=X(\xi)Y(\eta)\exp(\pm im\varphi)/\sqrt{\xi\eta}$, we obtain the following differential equations with respect to the variables $\tilde{\xi}$ and u:

$$\frac{d^2X}{d\tilde{\xi}^2}+P^2(b,\tilde{\lambda}_\xi,\alpha,\tilde{F};\tilde{\xi})X=0, \tag{2.4a}$$

$$\frac{d^2Y}{du^2}+Q^2(b,\delta,\alpha,\tilde{F};u)Y=0, \tag{2.4b}$$

where $P^2=-b^2p^2(\tilde{\xi})/4+b\tilde{\lambda}_\xi/\tilde{\xi}+(1-m^2)/4\tilde{\xi}^2$ and $Q^2=b^2h(u,d)-b\delta/4d+(1-4m^2)/4u^2$. By p^2 and h we denoted the following functions:

$$p^2=1+\tilde{F}\tilde{\xi}, \tag{2.5a}$$

$$h=\frac{1}{4d}-u^2+\frac{u^2(u^2-\bar{u}^2)}{(1-\alpha u^2)(1-\alpha u^2/2)}+\tilde{F}u^4, \tag{2.5b}$$

where $\tilde{F}=2FR^2/(Z-1/4)$ and $\bar{u}^2=(Z-1/2)/(Z-1/4)\alpha$. The quantity d in Eqs. (2.4b) and (2.5b) is introduced for convenience; it can be determined from the condition $h(u_0,d)=0$, where u_0 is the position of minimum of the function h, i.e., $h'(u_0,d)=0$. For given d and Z, the quantity h is a function of α and $\tilde{F}$.

The quantities $\tilde{\lambda}_\xi$ and δ in Eqs. (2.4a) and (2.4b) are spectral parameters (adapted to the critical region $R \approx R_c$) of effective one-dimensional eigenvalue problems along the $\tilde{\xi}$ and u axis. The parameter δ is defined by

$$\delta=b-16\tilde{\lambda}_\eta d, \tag{2.6}$$

where $\tilde{\lambda}_\eta$ is in relation with the spectral parameter $\tilde{\lambda}_\xi$ by the equation

$$(\tilde{\lambda}_\xi+\tilde{\lambda}_\eta)(-2\tilde{E}_\mu)^{1/2}=Z. \tag{2.7}$$

An important feature of the complex parameter δ is that it is very sensitive to the turning point configuration along the u direction. For that reason, it can be used to define the critical distance R_c. In the critical region we have $\delta(R)=\delta_0(R)+O(1/b)$. In the case of $R=R_c$, corresponding the confluence of the turning points, we have $\mathrm{Re}\,\delta_0(R_c)=0$. For $R>R_c$ and $R<R_c$, i.e., for the under-barrier and over-barrier transitions, the parameter $\mathrm{Re}\,\delta_0$ satisfies the inequalities $\mathrm{Re}\,\delta_0>0$ and $\mathrm{Re}\,\delta_0<0$, respectively. With the above definition, the parameter R_c has a somewhat similar role as that in the the classical over-barrier model [3].

C. Function ϵ and the ionization distance R_c^I

In the case of the electron tunneling in the vicinity of the potential barrier top, it is possible to obtain the analytical expressions for $\mathrm{Re}\,E_\mu(R)$ and $\Gamma_\mu(R)$ for a given set μ of parabolic quantum numbers as well as the parameters Z and F. Simultaneously, we obtain the spectral parameter $\delta=\delta(R)$.

Instead of $\delta(R)$, in the present paper we shall use a more convenient function $\epsilon(R)$, appearing as a spectral parameter in the etalon equation method (see the Introduction). What will be demonstrated in Sec. III A is the following relation between ϵ and δ:

$$\delta=\kappa\epsilon, \tag{2.8}$$

where $\kappa>0$ is a given constant. Consequently, up to the $O(1/b)$ term, we have

$$\mathrm{Re}\,\epsilon(R_c)=0, \tag{2.9}$$

so that $\mathrm{Re}\,\epsilon(R)>0$ for $R>R_c$, and $\mathrm{Re}\,\epsilon(R)<0$ for $R<R_c$. The relation (2.8) reflects the proportionality in the distances between turning points of the original and etalon equations, for the close turning point configuration.

In order to relate the ionization distance R_c^I and the function $\mathrm{Re}\,\epsilon$ we assume that the ionization probability $P_\mu(R)$ is determined by the rate equation $dP_\mu/dt=\Gamma_\mu(R)[1-P_\mu(R)]$. The solution of this equation, satisfying the condition $P_\mu(\infty)=0$, is given by

$$P_\mu(R)=1-\exp\left(-\frac{1}{v_\perp}\int_R^\infty \Gamma_\mu(R)dR\right). \tag{2.10}$$

The ionization distance $R=R_c^I$ is defined as a position of maximum of the total ionization rate $\tilde{\Gamma}_\mu(R)=dP_\mu/dt$; see Fig. 1(b). Accordingly, we have $d^2P_\mu/dR^2=0$ for $R=R_c^I$. By inserting Eq. (2.10) in the last expression we get

$$\left(\frac{d\Gamma_\mu}{dR}\right)_{R_c^I}+\frac{1}{v_\perp}\Gamma_\mu^2(R_c^I)=0. \tag{2.11}$$

Using the expansion $\Gamma_\mu(R)=\Gamma_\mu(R_c)+(\partial\Gamma_\mu/\partial\,\mathrm{Re}\,\epsilon)_{R^I}\mathrm{Re}\,\epsilon+O[(\mathrm{Re}\,\epsilon)^2]$, which is valid for $R \approx R_c \approx R_c^I$ when $|\mathrm{Re}\,\epsilon| \ll 1$, from Eq. (2.11) we obtain

$$\mathrm{Re}\,\epsilon(\mu,R_c^I,Z,F) \approx \epsilon_0(\mu,v_\perp,Z,F), \tag{2.12a}$$

where

$$\epsilon_0=-\frac{1}{\left(\frac{\partial \ln\Gamma_\mu}{\partial\,\mathrm{Re}\,\epsilon}\right)_{R_c}}-\sqrt{-\frac{v_\perp}{\left(\frac{\partial\Gamma_\mu}{\partial\,\mathrm{Re}\,\epsilon}\right)_{R_c}}\left(\frac{d\,\mathrm{Re}\,\epsilon}{dR}\right)_{R_c}}. \tag{2.12b}$$

In writing the last expression we took into account that $(d\,\mathrm{Re}\,\epsilon/dR)_{R_c^I} \approx (d\,\mathrm{Re}\,\epsilon/dR)_{R_c}$ because of the almost linear

behavior of Re ϵ in the vicinity of R_c, see Figs. 3–8 in Sec. IV.

Using the analytical form for the ionization rate in Eq. (2.12b), we calculate the function ϵ_0. With the known ϵ_0, Eq. (2.12a) gives an approximate expression for the ionization distance. A more exact expression for R_c^I follows directly from the numerical treatment of the relation (2.11); see Sec. IV.

III. IONIZATION DYNAMICS

A. Etalon equation method for $R \approx R_c$

The one-dimensional effective eigenvalue problems (2.4a) and (2.4b), with the variables $\tilde{\xi}$ and u, describe the finite and semi-infinite electron motions, respectively. Formally, Eq. (2.4a) has a form of a $\tilde{\xi}$ component of the standard Stark problem in parabolic coordinates. Equation (2.4b) expresses a specific feature of surface ionization for $R \approx R_c$ because the tunneling process in the vicinity of the effective potential barrier top takes place along the u axis.

Both these equations can be solved within the framework of the etalon equation method. However, while Eq. (2.4a) is tractable by the standard etalon equation procedure [20,21] and will not be considered in detail here, the solving of Eq. (2.4b) requires the particular methodology used in Refs. [23,24]. The two similar ionization problems have previously been analyzed by this approach: the ionization of an atomic particle in the critical electric field [23] and in the Coulomb field of the ionic projectile [24].

According to the etalon equation method (see the Introduction), the appropriate etalon equation of the problem (2.4a) is the Whittaker differential equation. Hence the solution $X(\tilde{\xi})$, satisfying the boundary conditions $X \to 0$ for $\tilde{\xi} \to 0$ and $\tilde{\xi} \to \infty$, can be expressed in terms of the Whittaker function $M_{a,b}(z)$, i.e., we have $X = KM_{\lambda_\xi, m/2}(b\mu)/\sqrt{\mu'}$, where K is a constant and $\lambda_\xi = n_1 + (m+1)/2$. We denote by $\mu = \mu(\tilde{\xi})$ a new "etalon" variable, and $\mu' = d\mu/d\tilde{\xi}$. Expanding the variable μ and spectral parameter $\tilde{\lambda}_\xi$ of Eq. (2.4a) in asymptotic series in terms of inverse powers of the large parameter b, we can obtain these quantities with arbitrary precision. For further calculations we need only the following relation:

$$\tilde{\lambda}_\xi = \lambda_\xi + (3\lambda_\xi^2 + \tau)\frac{\tilde{F}}{2b} + O\left(\frac{1}{b^2}\right), \tag{3.1}$$

where $\tau = (1-m^2)/4$; see, for example, Ref. [15], Sec. III B.

Equation (2.4b) has two close turning points, u_1 and u_2, determined by the condition $Q^2(b, \delta, \alpha, \tilde{F}; u_{1,2}) = 0$. For $u_1 \approx u_2$, the etalon equation method is significantly different in comparison to the distant turning point case, previously used in our analysis of the Rydberg level population of multiply charged ions at solid surfaces [15]. Namely, if $u_1 \approx u_2$, it is not possible to define the regions encompassing separately the points u_1 and u_2. Instead, we have to consider the region $\mathcal{A}_1$ far from the points $u_1 \approx u_2$, but which contains the point $u=0$, as well as the region $\mathcal{A}_2$ containing both turning points, but which is sufficiently far from the coordinate origin $u=0$ [23].

The etalon equation method of solving Eq. (2.4b), with the boundary conditions

$$Y(0) = 0,\ Y(u) = \text{outgoing wave},\ u > u_2, \tag{3.2}$$

adapted for $u_1 \approx u_2$, consists of choosing appropriate etalon equations in the regions $\mathcal{A}_1$ and $\mathcal{A}_2$ that have the same configuration of transitions points as in Eq. (2.4b). Note that the second condition in Eq. (3.2) is determined by the function $Y(u)$ in the region $\mathcal{A}_2$; accordingly, the condition is not dependent on the potential inside the solid. Also, the singularity of the potential U_M at $z=0$ does not affect this boundary condition. Besides, the supposition on the outgoing wave behavior of $Y(u)$ for $u > u_2$ along the u axis differs from the Siegert's diverging boundary condition used in CSM [7–9,19].

In the region $\mathcal{A}_1$, an appropriate etalon equation is the Bessel-type differential equation

$$\frac{d^2W}{d\nu^2} + \left(1 + \frac{1-4m^2}{4\nu^2}\right)W = 0, \tag{3.3}$$

with the etalon variable ν. The solution of Eq. (3.3) is given by $W(\nu) = C\sqrt{\nu}J_m(\nu)$, where $J_m(\nu)$ is the Bessel function, and C is a constant. The variable ν is related to the u variable, i.e., $\nu = \nu(u)$. The concrete form of this relation can be obtained by expanding the variable ν in the asymptotic series in terms of the large parameter b: $\nu(u) = \nu_1(u)b + \nu_0(u) + O(1/b)$. In the considered region $\mathcal{A}_1$, the solution $Y_1(u)$ of Eq. (2.4b) is expressed via the etalon equation solution $W(\nu)$ by the relation $Y_1(u) = W(\nu)/\sqrt{\nu'}$, where $\nu' = d\nu/du$.

On the other hand, in the region $\mathcal{A}_2$ an appropriate etalon equation is the Weber equation:

$$\frac{d^2U}{ds^2} + (s^2 - \epsilon)U = 0, \tag{3.4}$$

where $s = s(u)$ is the etalon variable in the $\mathcal{A}_2$ region and ϵ is the etalon spectral parameter for that region. Note that the parameter ϵ also represents a measure of the distance between turning points s_1 and s_2 of Eq. (3.4). We recall that ϵ is a suitable parameter for the derivation of the ionization distance R_c^I, Eq. (2.12a). By comparing the original equation (2.4b) and the etalon equation (3.4), we get the condition $s_{1,2} = s(u_{1,2})$, where $u_{1,2}$ are the turning points of Eq. (2.4b). Taking into account that $s_{1,2}^2 = \epsilon$, we have

$$\epsilon = s^2(u_{1,2}). \tag{3.5}$$

The general solution $U(s)$ of Eq. (3.4) is a linear combination of the functions of parabolic cylinder: $U(s) = AD_{-1/2+i\epsilon/2}(\sqrt{2}se^{-i3\pi/4}) + BD_{-1/2-i\epsilon/2}(\sqrt{2}se^{i3\pi/4})$, where A and B are constants. According to the etalon equation method, we have the asymptotic series $s^2(u) = w_1(u)b + w_0(u) + O(1/b)$. The solution Y_2 of Eq. (2.4b) in the region $\mathcal{A}_2$ is given by $Y_2 = U(s)/\sqrt{s'}$, where $s' = ds/du$.

By inserting the solutions Y_1 and Y_2 in Eq. (2.4b) and equating the coefficients with the same power of b, we obtain systems of the first-order nonlinear differential equations for

ν_i and w_i, $i=0,1$. The system of equations for w_i can be solved uniquely in each point of the u interval, including the position u_0 of minimum of the function h, Eq. (2.5b), only if the condition $\delta=\kappa\epsilon$ is satisfied, where $\kappa=2\sqrt{2h''(u_0)}d$. The proportionality of the parameters δ and ϵ has already been used in Eq. (2.8), from which we obtained $\mathrm{Re}\,\epsilon(R_c)=0$. By means of the relation $\delta=\kappa\epsilon$, together with the condition (3.5), we obtain the expansion coefficients ν_i and w_i, i.e., we calculate the functions $\nu(u)$ and $s^2(u)$ up to the terms of order $O(1/b)$. Using these functions as arguments in the etalon solutions, we arrive at the functions Y_1 and Y_2 of the original equation (2.4b) in the regions $\mathcal{A}_1$ and $\mathcal{A}_2$, respectively.

The functions $Y_1(u)$ and $Y_2(u)$ must be smoothly matched in the region $\mathcal{A}_1\cap\mathcal{A}_2$. From the matching condition $Y_1/Y_1'=Y_2/Y_2'$, using the asymptotic forms of the solutions Y_1 and Y_2, we get

$$A=B\exp\left[iD(b,\epsilon,\alpha,\tilde{F})-im\pi-i\pi/4+O\left(\frac{1}{b}\right)\right], \tag{3.6a}$$

where $D(b,\epsilon,\alpha,\tilde{F})$ is a given function of the complex parameters b, ϵ, α, and $\tilde{F}$. We have

$$D(b,\epsilon,\alpha,\tilde{F})=-2b\int_0^{u_1}h^{1/2}du+\epsilon\left[1+\frac{\kappa}{4d}\int_0^{u_1}h^{-1/2}du-\frac{1}{2}\ln\left(-4b\int_{u_1}^{u_0}h^{1/2}du\right)\right]. \tag{3.6b}$$

The asymptotic form of the solution $Y_2(u)$ for $u\gg u_2$ is a sum of two terms representing the incoming and outgoing waves along the u direction. The radiative condition, i.e., the second boundary condition from Eq. (3.2), will be satisfied if the amplitude of the incoming wave is equal to zero. As a consequence, besides Eq. (3.6a), we get an additional relation between the constants A and B:

$$A=B\frac{\sqrt{2\pi}}{\Gamma\left(\frac{1+i\epsilon}{2}\right)}\exp\left(-\frac{5\pi i}{4}-\frac{\pi\epsilon}{4}\right), \tag{3.7}$$

where $\Gamma(z)$ denotes the gamma function.

From Eqs. (3.6a) and (3.7) we obtain the following "dispersion" relation:

$$\exp\left[iD(b,\epsilon,\alpha,\tilde{F})-i(m-1)\pi+O\left(\frac{1}{b}\right)\right]=\frac{\sqrt{2\pi}}{\Gamma\left(\frac{1+i\epsilon}{2}\right)}\exp\left(-\frac{\pi}{4}\epsilon\right). \tag{3.8}$$

Under the condition $|\mathrm{Im}\,\epsilon|\ll 1$, Eq. (3.8) transforms into the following system of two real equations:

$$\mathrm{Re}\,D=\pi(2n_2+m+1)-\arg\Gamma\left(\frac{1+i\,\mathrm{Re}\,\epsilon}{2}\right) \tag{3.9a}$$

$$-\mathrm{Im}\,D-\frac{1}{2}\mathrm{Im}\,\epsilon\,\mathrm{Re}\,\psi\left(\frac{1+i\,\mathrm{Re}\,\epsilon}{2}\right)=\frac{1}{2}\ln[1+\exp(-\pi\,\mathrm{Re}\,\epsilon)], \tag{3.9b}$$

where $\psi(z)=d\ln\Gamma(z)/dz$ represents the digamma function of the complex variable z.

The system of Eqs. (3.9a) and (3.9b) represents a mathematical background of our description of the ionization dynamics at $R\approx R_c$. Namely, this system of equations enables us to obtain the energies and ionization rates of the active electron, as well as the function $\mathrm{Re}\,\epsilon$ necessary for determining the ionization distances R_c^I and the critical distances R_c. Note that these physically relevant quantities will not be expressed in terms of the volume CSM integrals, but by "etalon-method integrals," figuring in Eq. (3.6b) and, accordingly, contained in Eqs. (3.9a) and (3.9b). The most important feature of these integrals, from the standpoint of the etalon equation method, is that they are not sensitive to the form of electronic potential in the near-surface region ($z\approx 0$).

B. Explicit expressions for the functions $\mathrm{Re}\,\epsilon$, Γ_μ, and $\mathrm{Re}\,\tilde{E}_\mu$

The obtaining of explicit expressions for the R-dependent functions $\mathrm{Re}\,\epsilon$, Γ_μ, and $\mathrm{Re}\,\tilde{E}_\mu$ is possible through the following procedure. For a given R, we determine $\mathrm{Re}\,D$ and $\mathrm{Im}\,D$ by using Eq. (3.6b). Inserting these expressions into Eqs. (3.9a) and (3.9b) we arrive at the relations for $\mathrm{Re}\,\epsilon$ and Γ_μ, respectively. Thus the quantities $\mathrm{Re}\,\epsilon$ and Γ_μ are expressed in terms of $\mathrm{Re}\,E_\mu$. The function $\mathrm{Re}\,E_\mu$ can be obtained by using Eqs. (2.6) and (2.8), as well as Eqs. (2.7) and (3.1).

According to this general scheme we obtain the following system of equations for the variables $\mathrm{Re}\,\epsilon$, Γ_μ and $\mathrm{Re}\,\tilde{E}_\mu$:

$$\mathrm{Re}\,\epsilon=\frac{f_1\mathrm{Re}\,b+2\pi(2n_2+m+1)}{f_2-\ln(\mathrm{Re}\,b)}\left[1+O\left(\frac{1}{b}\right)\right], \tag{3.10a}$$

$$\Gamma_\mu=\frac{-2\,\mathrm{Re}\,\tilde{E}_\mu}{\mathrm{Re}\,b}\frac{\ln(1+\exp(-\pi\,\mathrm{Re}\,\epsilon))}{[\ln(\mathrm{Re}\,b)-f_2]\left(a_1+\frac{a_2}{\mathrm{Re}\,b}\right)+f_3+O\left(\frac{\ln b}{b^2}\right)}, \tag{3.10b}$$

$$\mathrm{Re}\,\tilde{E}_\mu=-\frac{Z^2}{2}\left[\mathrm{Re}\,\tilde{\lambda}_\xi+\frac{\mathrm{Re}\,b}{16\,\mathrm{Re}\,d}-a_3\mathrm{Re}\,\epsilon+O\left(\frac{1}{b^2}\right)\right]^{-2}, \tag{3.10c}$$

where $\mathrm{Re}\,b=2(-2\,\mathrm{Re}\,\tilde{E}_\mu)^{3/2}R^2/(Z-1/4)$. The quantity $\mathrm{Re}\,\tilde{\lambda}_\xi$ from Eq. (3.10c) is given by Eq. (3.1), where b is replaced by $\mathrm{Re}\,b$.

The functions f_1 and f_2, figuring in Eqs. (3.10a) and (3.10b), are defined by the following integrals:

$$f_1=4\,\mathrm{Re}\int_0^{u_0}h^{1/2}du, \tag{3.11a}$$

and

$$f_2 = 2\sqrt{2}\mathrm{Re}\left(\beta\int_0^{u_0} h_r^{-1/2}du\right) - \ln|2\sqrt{2}\beta u_0^2| + \psi(1/2), \tag{3.11b}$$

where $h_r^{-1/2}=h^{-1/2}-1/\beta\sqrt{2}(u-u_0)$ is the regular part of the function $h^{-1/2}$ and $\beta=\sqrt{h''(u_0,d)}/2$. We recall that the quantities u_0 and d are defined in Sec. II B; see the text followed by Eq. (2.5b). By $\psi(1/2)$ we denoted the value of the digamma function for $z=1/2$. The function f_3 is defined by

$$f_3 = \frac{3}{2}f_1 + \left(\alpha\frac{df_1}{d\alpha}\right)_{\alpha=\mathrm{Re}\ \alpha}. \tag{3.11c}$$

In Eqs. (3.10b) and (3.10c) we denoted by a_i, $i=1$, 2, and 3, the smoothly varying functions of the parameters b, ϵ, α, and $\tilde{F}$. Explicit expressions of the quantities a_i and Re d, as well as the expressions for f_i, $i=1$, 2, and 3, are given in the Appendix.

From Eqs. (3.10a), (3.10b), and (3.10c) we see that the quantities Re $\epsilon(R)$, $\Gamma_\mu(R)$, and Re $\tilde{E}_\mu(R)$ must be determined simultaneously; this is characteristic for the etalon equation method when solving the quasistationary eigenvalue problem for $R\approx R_c$. Bearing in mind that f_i, a_i, and Re d represent the known functions of Re $\tilde{E}_\mu$ (see the Appendix), the numerical treatment of the system (3.10a), (3.10b), and (3.10c) becomes relatively simple. Namely, Eqs. (3.10a) and (3.10c) have the following structure: Re $\epsilon=\mathcal{F}_1(\mathrm{Re}\,\tilde{E}_\mu)$ and Re $\tilde{E}_\mu=\mathcal{F}_3(\mathrm{Re}\,\epsilon,\mathrm{Re}\,\tilde{E}_\mu)$, where $\mathcal{F}_1$ and $\mathcal{F}_3$ represent known nonlinear functions of the variables indicated. Accordingly, for Re $\tilde{E}_\mu$ we get the transcendental equation Re $\tilde{E}_\mu=\mathcal{F}_3(\mathcal{F}_1(\mathrm{Re}\,\tilde{E}_\mu),\mathrm{Re}\,\tilde{E}_\mu)$, which can be easily solved numerically for any relevant value of R. With the known Re $\tilde{E}_\mu$, we return to Eq. (3.10a) and calculate Re ϵ. Finally, Eq. (3.10b) has the following structure: $\Gamma_\mu=\mathcal{F}_2(\mathrm{Re}\,\epsilon,\mathrm{Re}\,\tilde{E}_\mu)$, where $\mathcal{F}_2$ is the known nonlinear function of the Re ϵ and Re $\tilde{E}_\mu$. Consequently, with the known Re ϵ and Re $\tilde{E}_\mu$, we arrive to the ionization rate Γ_μ. In this way we obtain the R-dependent functions Re $\epsilon(R)$, $\Gamma_\mu(R)$, and Re $\tilde{E}_\mu(R)$. Of course, these results are valid in the physically most relevant region around the $R=R_c$; we have focused on this region from the very beginning of our analysis.

In the far asymptotic region, i.e., for $R\gg R_c\gg 1$, we have a deep sub-barrier tunneling; in that case the surface potential U_M+U_{AM} is given by Eq. (2.2b). The corresponding energy eigenvalue problem overcomes into the Stark-like one with the (shifted) eigenenergies denoted by $\tilde{E}_{0,\mu}$. For the hydrogenlike atom (core charge Z) in a weak electric field F, satisfying the condition $n^2F\ll 1$, we have

$$\tilde{E}_{0,\mu} \approx -\frac{Z^2}{2n^2} + \frac{3}{2Z}Fn(n_1-n_2) + \frac{2Z-1}{4R} - \frac{3}{8}\frac{(Z-1)}{ZR^2}n(n_1-n_2). \tag{3.12}$$

In the absence of the field, the energies $\tilde{E}_{0,\mu}$ turn into the hydrogenlike energies $E_0=-Z^2/2n^2$ when $R\to\infty$.

C. Explicit form of the condition Re $\epsilon(R_c^I)=\epsilon_0$

The ionization distances R_c^I can be obtained approximately from Eq. (2.12a) providing that the function ϵ_0 is known. We calculate the quantity ϵ_0 using the relation (3.10b) for Γ_μ expressed in the form $\Gamma_\mu(R)=A(\mathrm{Re}\,\epsilon)\ln[1+\exp(-\pi\,\mathrm{Re}\,\epsilon)]$. Taking into account that Re $\epsilon(R_c)=0$, from Eq. (2.12b) we get

$$\epsilon_0 = \frac{2\ln 2}{\pi}\left[1+\chi-\sqrt{\frac{2\ln 2}{\pi}\left(\frac{d\,\mathrm{Re}\,\epsilon}{dR}\right)_{R_c}\frac{v_\perp}{\Gamma_\mu(R_c)}\frac{1}{1+\chi}}\right], \tag{3.13a}$$

where

$$\chi = \frac{\chi_0}{1-\chi_0}, \quad \chi_0 = \frac{2\ln 2}{\pi}\left(\frac{d\ln A}{d\,\mathrm{Re}\,\epsilon}\right)_{R_c}. \tag{3.13b}$$

Considering the function $A(\mathrm{Re}\,\epsilon)$ as a smoothly varying function of Re ϵ, we have $\chi\approx 0$. Furthermore, for the velocities $v_\perp\approx 10^{-5}$ a.u. relevant in the experiment [1], the third term in Eq. (3.13a) is also a small quantity. As a result, we get

$$\mathrm{Re}\,\epsilon(R_c^I) \approx \epsilon_0 \approx \frac{2\ln 2}{\pi}, \tag{3.14}$$

i.e., we obtain an approximative, but simple, equation for determining the ionization distances R_c^I from the known graphs for Re $\epsilon(R)$.

Let us note that the quantity ϵ_0, Eq. (3.13a), increases with the decreasing of the velocity $v_\perp$, which results in an increasing of the ionization distances R_c^I.

IV. RESULTS

A. Energies and ionization rates for $R\approx R_c$

From the results presented in Sec. III, various quantitative details concerning the ionization dynamics around the critical ion-surface distances $R\approx R_c$ can be explicated.

In Fig. 3 we present the relevant physical quantities in the case of ionization of the hydrogen atom ($Z=1$) states with $n=8$, 12, 16, and 20, and for $n_1=0$ and $m=0$ in the absence of electric field ($F=0$). Figure 3(a) exposes the function Re $\epsilon(R)$ whose zeros are the critical distances R_c [circles in Fig. 3(a)]. The corresponding ionization distances R_c^I [dots in Fig. 3(a)] are obtained as intersections of the curve Re $\epsilon(R)$ with Re $\epsilon=\epsilon_0$, see Eq. (3.14). We see that the ionization distances R_c^I are localized in the vicinity of R_c. Taking into account that $R_c^I-R_c>0$, we conclude that the ionization is mainly a tunneling process. With the increasing of n the ionization distances increase following the quadratic law. A more detailed analysis of the quantity R_c^I as a function of n is given in Sec. IV B.

In Figs. 3(b) and 3(c) we present, respectively, the ionization rates and the (shifted) energy terms Re $\tilde{E}_\mu=\mathrm{Re}\,E_\mu-FR$ (solid curves) for the electron transitions in the vicinity of the potential barrier top. In Fig. 3(c) we also expose the (shifted) energies $\tilde{E}_{0,\mu}$ (dot-dashed curves) given by Eq.

(3.12), valid for $R \gg R_c$, i.e., in the case of deep sub-barrier electron tunneling. In the critical region $R \approx R_c$ the energy terms $\mathrm{Re}\,\tilde{E}_\mu$ increase with the increasing of R; in the far asymptotic region $R \gg R_c$, the terms $\tilde{E}_{0,\mu}$ have a decreasing character. The energy terms from the critical region and from the far asymptotic region intersect at ion-surface distances larger that R_c^I. A unique energy curve can be constructed as a combination of the two types of curves presented in Fig. 3(c).

The influence of the external electric field is illustrated in Fig. 4, in which we consider the ionization of hydrogenic ($Z=1$) Rydberg state $n=10$, $n_1=0$, $m=0$ for the electric fields $F_1=0$, $F_3=1.0\times10^{-6}$ a.u., and $F_5=2.0\times10^{-6}$ a.u. In Fig. 4(a) we present the function $\mathrm{Re}\,\epsilon(R)$ for the electric fields $F=F_1$, F_3, and F_5. The ionization distances R_c^I (marked by dots), mainly localized at $R_c^I \approx 340$ a.u., are very close to the critical distances R_c (circles) and they slightly increase with the increasing of F.

In Figs. 4(b) and 4(c) we present the ionization rates $\Gamma_\mu(R)$ and the shifted energies $\mathrm{Re}\,\tilde{E}_\mu(R)$ obtained in the critical region $R \approx R_c$, as well as asymptotic energies $\tilde{E}_{0,\mu}(R)$, determined by Eq. (3.12). In the same figures we present the corresponding theoretical rates and energies [9,18,19] obtained within the framework of the CSM. In order to compare the cited results with our parabolic energies and rates with $n_1=0$, we present the curves from Refs. [9,18,19] for the shortest lived states. The ordering of the CSM-curves in Figs. 4(b) and 4(c) is the same as that of solid curves. From Fig. 4(b) we see that the rates $\Gamma_\mu(R)$ obtained in our model follow the CSM curves almost over the entire R region. The coinciding of these curves is most notable for $R \approx R_c^I$, dots in Fig. 4(b). We obtain the same agreement by comparing our rates for $Z=1$, $n=13$, $n_1=0$, and $m=0$ with the CSM rates taken from Ref. [1] for $H(n=13)$ the "reddest" $m=0$ state.

From Fig. 4(c) we conclude that, in the region of validity of our model ($R \approx R_c$), the energy terms $\mathrm{Re}\,\tilde{E}_\mu(R)$ obtained here (solid curves) and the CSM terms [9,19,18] (dashed curves) have the same characteristic increasing behavior with the increasing of R. Outside the mentioned critical region, for larger R, the terms from the cited references are in agreement with the asymptotic terms (dot-dashed curves). On the other hand, outside the critical region, and for smaller R, the energy terms $\mathrm{Re}\,\tilde{E}_\mu(R)$ and those from CSM have the same increasing behaviors with the decreasing of R. However, our curves, extrapolated from the critical region, are shifted towards smaller R in comparison to CSM curves. Of course, in the region $R \ll R_c$, we are in the far over-barrier region. In this case, the turning points are distant and localized in the complex plane, so that the main assumptions of our model are no longer valid; the energy terms from this region are irrelevant for the calculation of ionization distances $R_c^I \approx R_c$.

In Fig. 5 we present the same quantities as in Fig. 4, but for the hydrogenic Rydberg state $n=15$. The general behaviors of the function $\mathrm{Re}\,\epsilon$, energies and rates are the same as in Fig. 4, except the effect of the field F is more pronounced. The obtained values are compared with the theoretical results of CSM [22] corresponding to the hydrogenic case in which the states of the considered manifold are fully hybridized.

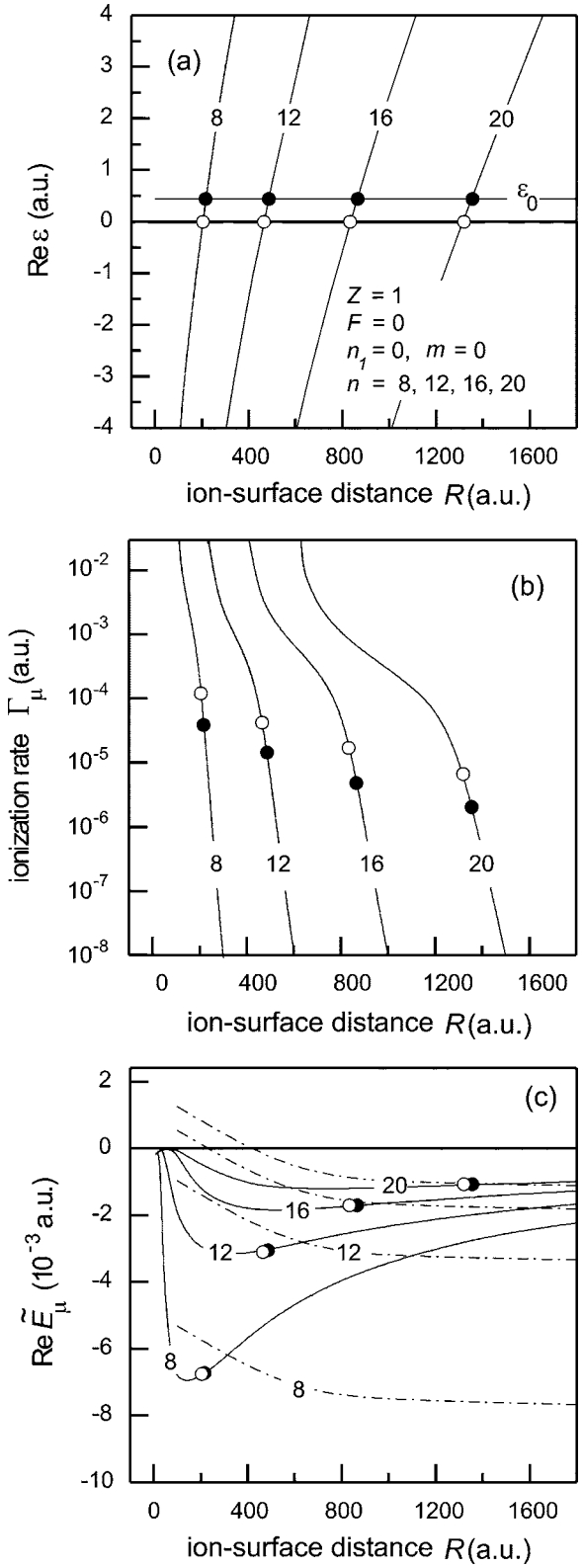

FIG. 3. Ionization of the hydrogenic ($Z=1$) Rydberg states $n=8$, 12, 16, and 20 in the absence of electric field ($F=0$); (a) the function $\mathrm{Re}\,\epsilon(R)$, (b) ionization rates $\Gamma_\mu(R)$, and (c) shifted energies $\mathrm{Re}\,\tilde{E}_\mu(R)$ (solid curves) and $\tilde{E}_{0,\mu}(R)$ (dot-dashed curves). Dots and circles indicate the positions of ionization distances R_c^I and critical distances R_c, respectively.

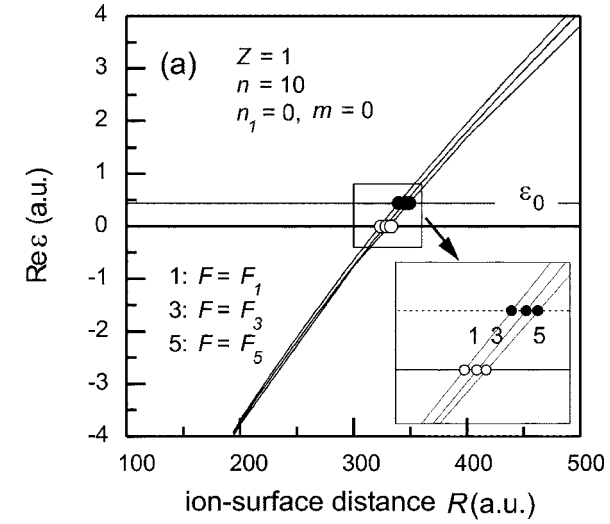

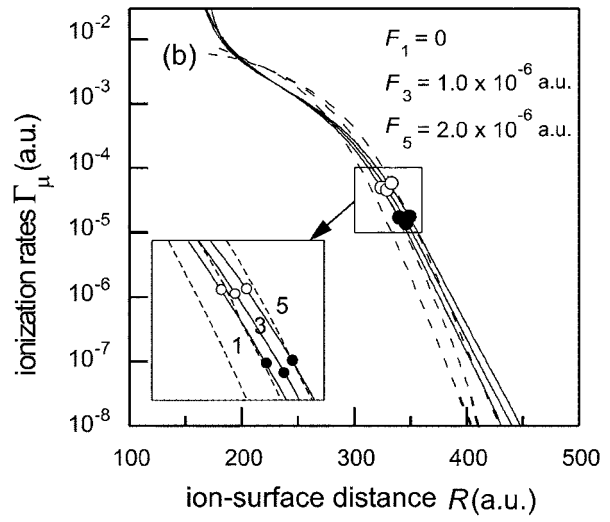

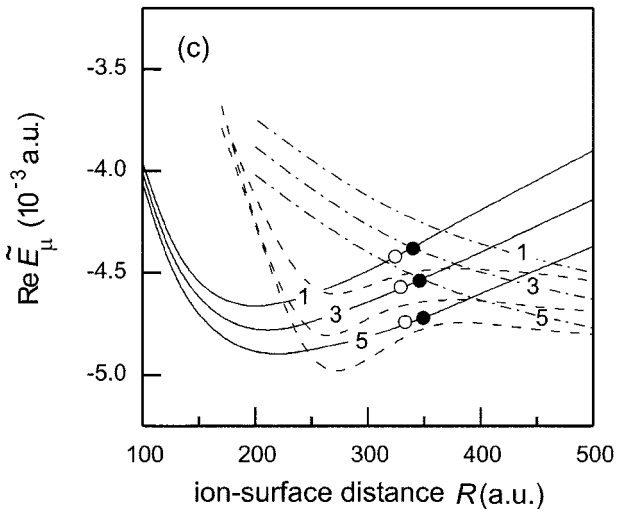

FIG. 4. (a) The function Re $\epsilon(R)$, (b) the ionization rates $\Gamma_\mu(R)$, and (c) the energies Re $\tilde{E}_\mu(R)$ (solid curves) and $\tilde{E}_{0,\mu}(R)$ (dot-dashed curves) of the state $n=10$, $n_1=0$, $m=0$ in the electric fields F_1, F_3, and F_5. Dots and circles indicate the positions of R_c^I and R_c, respectively. Dashed curves are the CSM results from Ref. [19] (or Ref. [18]) for $F=F_3$ and $F=F_5$, and from Ref. [9] for $F=F_1=0$.

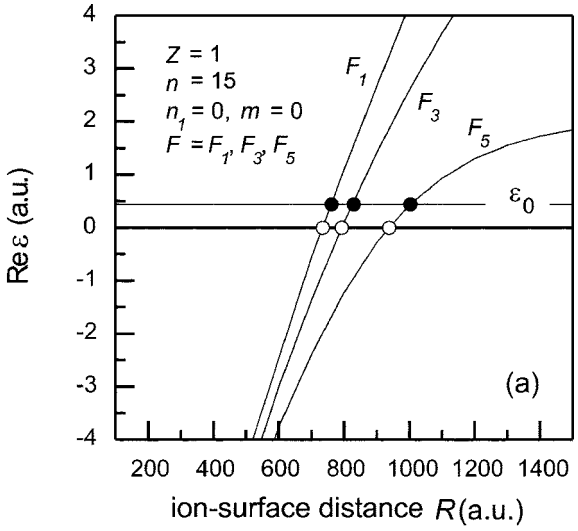

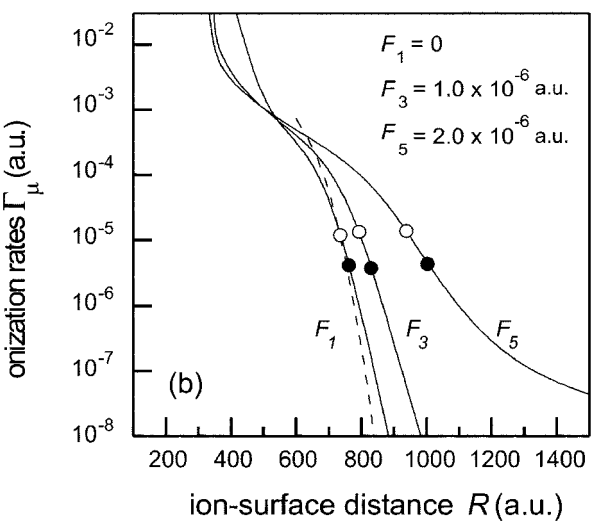

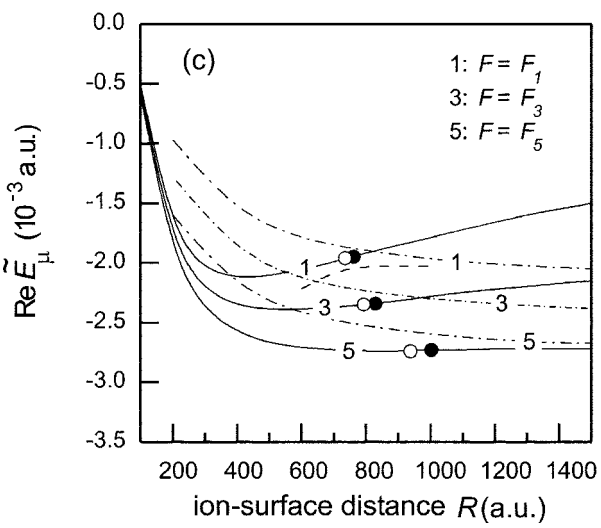

FIG. 5. (a) The function Re $\epsilon(R)$, (b) the ionization rates $\Gamma_\mu(R)$, and (c) the energies Re $\tilde{E}_\mu(R)$ (solid curves) and $\tilde{E}_{0,\mu}(R)$ (dot-dashed curves) of the hydrogenic state $n=15$, $n_1=0$, $m=0$ in the electric fields F_1, F_3, and F_5. Dots and circles indicate the positions of R_c^I and R_c, respectively. Dashed curves are the CSM results for $F=F_1=0$; see Fig. 1(b) in Ref. [22].

The comparison of our curves and those of CSM leads to the same conclusion as in the case of $n=10$ discussed in Fig. 4. Namely, the agreement of the rates exists almost over the entire region of the R axis; the energies $\mathrm{Re}\,\tilde{E}_{\mu}(R)$, solid curve 1, and $\tilde{E}_{0,\mu}(R)$, dot-dashed curve 1, constitute a unique curve in agreement with the energy term of Ref. [22] (dashed curve).

In Fig. 6 we illustrate the situation in the parabolic manifold of a given n and m. We consider the Rydberg state $n=10$, $m=0$ in the field $F_3=1.0\times10^{-6}$ a.u. restricting ourselves to the low values of n_1 ($n_1=0$, 1, and 2). In Fig. 6(a) we present the function Re ϵ by indicating the corresponding ionization distances R_c^I (dots) and critical distances R_c (circles). With the increasing of n_1, the R_c^I values decrease in agreement with the values obtained in Ref. [19] for $v_{\perp}=2.1\times10^{-5}$ a.u: $R_c^I\approx360$ a.u. for the shortest lived state and $R_c^I\approx120$ a.u. for the longest lived one; see also our discussion in Sec. IV B.

In Fig. 6(b) we present the ionization rates via the ion-surface distance R for $n_1=0,1,2$ and $m=0$. From the presented curves we conclude that (at a given ion-surface distance R) the Rydberg state with $n_1=0$ represents the shortest lived state, i.e., it gives the main contribution to the ionization process. On the other hand, considering the values of the ionization rates at $R=R_c^I$ [dots in Fig 6(b)], we conclude that they are of the same order. The obtained rates are compared with the theoretical CSM results [19]; we present only the three largest rates from the manifold obtained in cited reference. Our predictions are in agreement with those of Ref. [19].

The parabolic energy manifolds $\mathrm{Re}\,\tilde{E}_{\mu}=\mathrm{Re}\,E_{\mu}(R)-FR$ from the critical region and $\tilde{E}_{0,\mu}(R)$ from the far asymptotic region, in the external field $F=F_3$, are presented in Fig. 6(c). In the same figure we also expose the lowest three terms of the theoretical CSM energies [19] (the ordering of the CSM curves is the same as that of solid curves). Note that, like in Figs. 4 and 5, the energy terms $\mathrm{Re}\,\tilde{E}_{\mu}$ obtained in the present paper and the terms from Ref. [19] have the same behavior for $R\approx R_c$ (circles). Again, the unique curves that can be constructed on the base of the critical and asymptotic values of the energies reproduce the CSM terms.

The energies and rates of the Rydberg states with different m can also be obtained from our model. Although less pronounced we found these behaviors to be similar to the ones in the above presented n_1 case. Some aspects of the m dependence of the ionization distances are discussed in Sec. IV B.

The results presented in Figs. 3–6 show that the rates and energy terms, for different n, n_1, and F, are in agreement with those of the complex scaling method almost over the entire R region. In this sense we conclude that the parabolic quantum numbers can be used as approximately good quantum numbers for a classification of the "Stark-like" states of the CSM approach [9,18,19,22], at least for lower n_1 values.

B. Ionization distances R_c^I and comparison with experiments

The most important output of our calculations concerns the ionization distances R_c^I which give basic physical information about the ionization process. In the model presented, the ionization distances depend on the set of parabolic quantum numbers $\mu=(n_1,n_2,m)$, where $n_1+n_2+|m|+1=n$. Be-

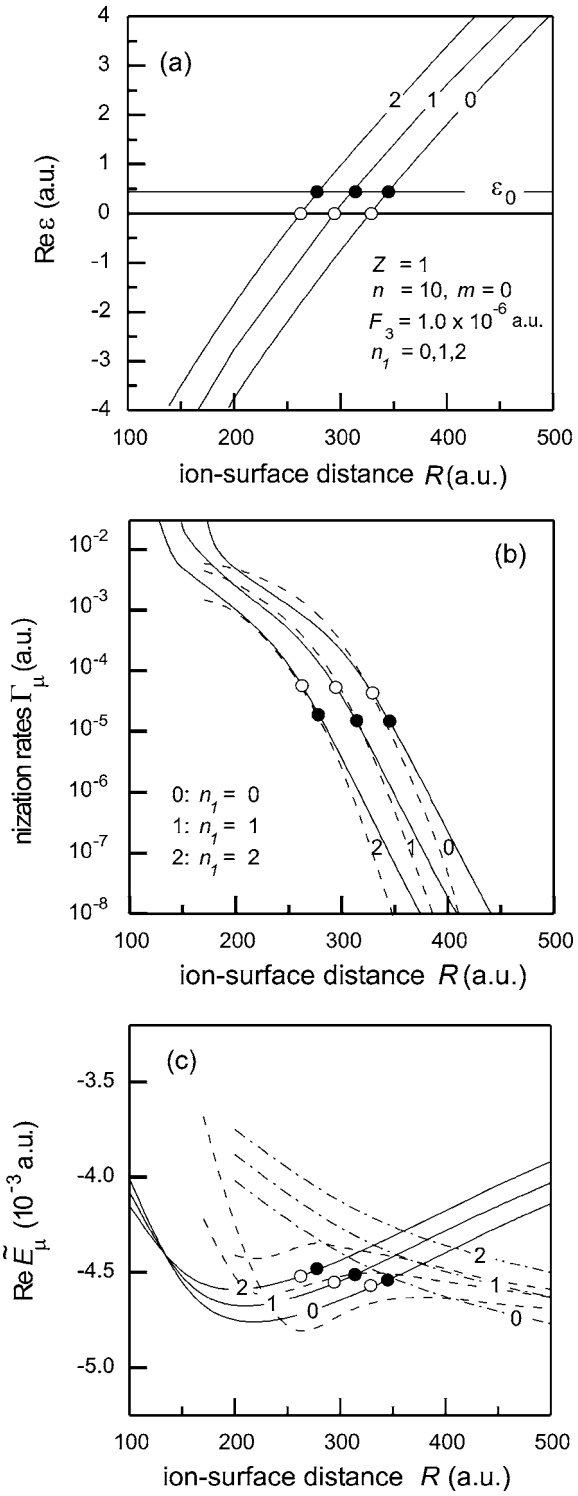

FIG. 6. (a) The function Re $\epsilon(R)$, (b) ionization rates $\Gamma_{\mu}(R)$, and (c) the parabolic energy manifolds $\mathrm{Re}\,\tilde{E}_{\mu}(R)$ (solid curves) and $\tilde{E}_{0,\mu}(R)$ (dot-dashed curves) of the state $n=10$, $m=0$ in the electric field $F=F_3$. Numbers indicate the values of n_1. Dots and circles indicate the positions of R_c^I and R_c, respectively. Dashed curves are the CSM results from Ref. [19].

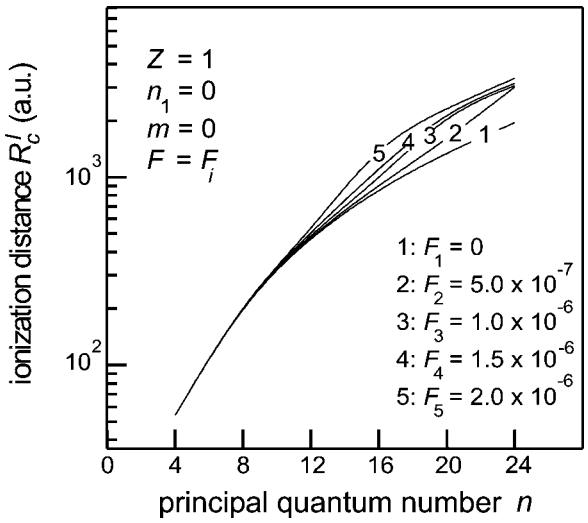

FIG. 7. The ionization distance R_c^I via principal quantum number n in the external electric field F; the values of the field are marked (in atomic units).

sides, the values of R_c^I depend on the ionic velocity $v_\perp$, the core charge Z, and the strength of the electric field F.

In the first approximation, the ionization distances are determined by Eq. (3.14), in which the velocity dependence is neglected. The corresponding data are sufficiently accurate for a discussion on the general behavior of the quantity R_c^I and for a comparison with the critical distance R_c. In Table I we present the R_c^I values, calculated by Eq. (3.14), for $n_1=0$, $m=0$, and the electric fields $F_1=0$, $F_2=5.0\times10^{-7}$, $F_3=1.0\times10^{-6}$, $F_4=1.5\times10^{-6}$, and $F_5=2.0\times10^{-6}$ (in atomic units). In Table II we consider two cases: the case $n=10$, $m=0$ for $n_1=0,1,2,\ldots 6$, and the case $n=10$, $n_1=0$ for $m=0,1,2,\ldots, 6$.

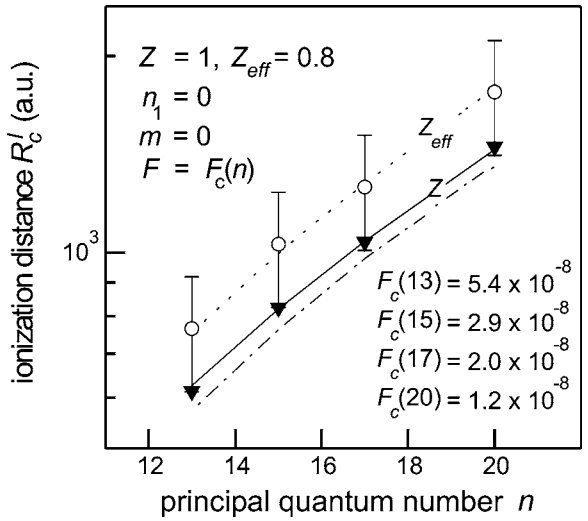

FIG. 8. The ionization distances R_c^I for $Z=1$ with the principal quantum number $n=13,15,17$, and 20 in the threshold external electric fields $F=F_c(n)$: the approximate (dot-dashed curve) and "exact" (solid curve) results, Eqs. (3.14) and (2.11), respectively. The values of the field $F_c(n)$ (in atomic units) are taken from the experiment [1]. Circles are the experimental data taken from Ref. [1]. Symbols (▼) are the CSM theoretical predictions according to Ref. [1]. The case $Z_{eff}=0.8$ is also presented (dotted curve).

TABLE I. The ionization distances R_c^I (in a.u.) according to Eq. (3.14). The cases of Rydberg state $(n,n_1=0,m=0)$ of the hydrogenic $(Z=1)$ atom in the external electric field $F_i, i=1,2,\ldots5$ are presented; the values of the field are given in the text.

n	4	8	12	16	20	24
$R_c^I(F_1)$	54	216	487	866	1356	1949
$R_c^I(F_2)$	54	216	493	907	1594	3024
$R_c^I(F_3)$	54	217	500	976	2202	3071
$R_c^I(F_4)$	54	218	510	1118	2255	3159
$R_c^I(F_5)$	54	218	519	1523	2339	3355

The trend we see in Tables I and II is the increasing of distance R_c^I with the increasing of principal quantum number n, scaled as n^2. The influence of other parameters on the R_c^I values is not so evident: in some cases we have an interplay of several different behaviors. In principle, the R_c^I values increase with the increasing of the electric field F, see Table I. In the absence of the field $(F=F_1=0)$, and for lower values of F, the ionization distances corresponding to a given n decrease with the increasing of the first parabolic quantum number n_1; see Table II. The influence of the quantum number m is similar, but less pronounced.

The obtained numerical results for R_c^I can be summarized by the following expression: $R_c^I=3.3f(\mu,v_\perp,Z,F)n^2/Z$. In the absence of the field F, for the hydrogenic case $(Z=1)$, from the approximative Eq. (3.14) we get $f=1$. The direct numerical calculation of the ionization distances on the base of Eq. (2.11), applied to the case $v_\perp \ll 1$, gives somewhat larger R_c^I values. Namely, in the absence of the field, for $Z=1$ and $v_\perp \approx 10^{-5}$ a.u., instead of $f=1$ we get $f=1.15$, i.e., we have $R_c^I \approx 3.8n^2$, in agreement with CSM results; see comments in Ref. [1]. Note that the classical over-barrier model [2] gives $R_c^I=R_c\approx 3n^2$. With the increasing of F, the value of function f increases; for the field $F=F_5$ and $n_1=0$, $m=0$ and for larger n we get $f=1.8$, i.e., $R_c^I\approx 6n^2$.

In Fig. 7 we present graphically the ionization distances R_c^I from Table I as a function of n, for different values of F indicated. We see that the curves corresponding to different values of $F\neq0$ represent the branches of the "basic" zero-field curve $(F=F_1=0)$. The branching becomes more pronounced with increasing of n. Under the experimental conditions, the ionization distance R_c^I for a given n corresponds to the threshold (critical) value of electric field, $F=F_c(n)$.

In Fig. 8 we present the ionization distances R_c^I for the Rydberg states with the principal quantum numbers $n=13$,

TABLE II. The ionization distances R_c^I (in a.u.) according to Eq. (3.14), for the state $n=10$, $m=0$ as a function of n_1 (first row), and $n=10$, $n_1=0$ as a function of m (second row). The value of the external electric field is given by $F_3=1.0\times10^{-6}$ a.u.

n_1 or m	0	1	2	3	4	5	6
$R_c^I(n_1)$	343	311	279	247	212	178	142
$R_c^I(m)$	342	327	311	295	279	262	246

15, 17, and 20 and the electric field $F=F_c(n)$, for which the experimental data [1] are available. Note that the $F_c(n)$ values correspond to the branches which are very close to the zero-field branch $F_1=0$ exposed in Fig. 7. The experiment was performed with the thermal beam of xenon Rydberg atoms in the near grazing incidence ($v_\perp=7\times10^{-6}$ a.u.) onto Au(111) surface. The ionization distances for the "reddest" $m=0$ states (the states mainly oriented towards the surface) of each Xe(n) "Stark manifold" have been measured. In our model, these states are labeled by the parabolic quantum numbers $n_1=0$, $m=0$. The experimental data [1] for the ionization distances are marked with circles. The theoretical (dot-dashed) curve obtained approximately in the present paper by Eq. (3.14) follows the law $R_c^I=3.3n^2$. On the other hand, for the velocity $v_\perp$ used in the experiment [1], direct numerical calculation of the ionization distance by Eq. (2.11) gives the solution (full line) that follows the law $R_c^I\approx3.8n^2$. In the same figure we present the results of CSM hydrogenic theory (symbols) reported in Ref. [1]: $R_c^I=3.8n^2$. The exact full-line solution presented is practically identical with the result of CSM. This agreement was expected because the rates calculated in the present paper (Sec. IV A) follow the complex scaling rates.

Strictly speaking, a direct comparison of the results presented here with the experimental data [1] is not possible because the experiment has been performed with Xe atoms which are unlike the hydrogen ones. An extension of ionization models from the hydrogenic to the Xe-case represents a nontrivial problem both within the framework of CSM and the etalon equation method. In CSM, an effort to resolve the problem has been made by including the quantum defects of free Xe atoms, using appropriate pseudopotentials [22]. These results, however, could not be taken as sufficiently conclusive; in particular, only the prediction for Xe($n=15$) has been reported, giving $R_c^I<700$ instead of the experimental value $R_c^I\approx1000$. The problem also remains open in the etalon equation method. It is peculiar that the presented hydrogenlike model with effective core charge $Z=Z_{eff}=0.8$ (estimated on the base of approximative calculation of R_c^I) reproduces formally the experimental data $R_c^I=(4.5\pm0.9)n^2$, see Fig. 8, dotted curve.

V. CONCLUDING REMARKS

In this paper we proposed a "tunneling model" of ionization of the hydrogenlike Rydberg atom in an external (weak) electric field. This model points out that a decisive role in the ionization process is that of the critical region $R\approx R_c\gg1$. For that reason, our etalon equation asymptotic procedure has been focused on that region of ion-surface distances R. The method offers sufficiently accurate analytical expressions for the rates $\Gamma_\mu(R)$ and energy terms Re $E_\mu(R)$, as well as the critical distances R_c and ionization distances R_c^I.

The main practical conclusion of the present paper is that the parabolic quantum numbers can be used as approximately good quantum numbers for a complete classification of the decaying states. Accordingly, the "reddest states" of CSM [22], can be identified with the parabolic state with $n_1=0$: the states numerated in Ref. [22] as second, third, etc. correspond to the parabolic quantum numbers $n_1=1$, $n_1=2$, etc., respectively. Note that the same conclusion, but for $F=0$ and multiply charged ions with lower values of n, has been obtained [6] by comparing the CAM method with the perturbation method.

Few additional concluding comments may be relevant for further investigations of the R_c^I problem.

First, the calculations exposed in Sec. III can be extended from the hydrogenic case ($Z=1$), to the case of arbitrary ions ($Z\neq1$) approaching to (or escaping from) solid surfaces. In particular, the values of the ionization rates and the R_c^I distances for $Z\gg1$ would be relevant. Besides, further elaboration of the concept of effective core charge $Z=Z_{eff}<1$ is possible. The concept of the effective core charge could rather be related with the external electric field effect than with recent estimations addressed to the isolated Xe^+ [22].

Second, the relevance of various members of a parabolic (Stark-like) manifold is still an open problem; the additional experiments [25] with xenon Rydberg atoms report that the "extreme red" and "extreme blue" states of the manifold are ionized at nearly the same distances R_c^I. A theoretical explanation, based on the avoided crossings between neighboring levels, calculated with the aid of CSM using the pseudopotentials, has been proposed in Ref. [26]. The results obtained in the present paper are not sufficiently accurate for large n_1 values ($n_1\approx n_{1,\max}=n-1$). The situation is somewhat similar to the case of large-l Rydberg states treated recently within the framework of the two-state population-reionization model [17]. Namely, in the large-n_1 case, like in the large-l case, a wide space region around the projectile trajectory could contribute to the electron exchange process. In that case, the approximation $\xi\ll\eta$ used in Sec. II A is not applicable, so that additional theoretical investigations are needed.

Third, within the framework of the two-state vector model [14–17] a generalized expression for the ionization distances R_c^I can be obtained. Namely, the two wave functions, $\Psi_\nu^{(1)}$ and $\Psi_\mu^{(2)}$, which simultaneously define the instant state of an active electron at intermediate stages of the ion-surface interaction, could be labeled by two different sets of quantum numbers ν and μ, respectively. Consequently, the ionization distances depend on two sets of quantum numbers, i.e., we have $R_c^I=R_c^I(\mu,\nu)$. For the ionization process discussed in the present paper, the appropriate sets of quantum numbers are the sets of spherical and parabolic quantum numbers. We expect that a new insight into the ionization process can be obtained from the behaviors of the $R_c^I(\mu,\nu)$ curves for a given n and m.

ACKNOWLEDGMENT

This work was supported in part by the Ministry of Science and Ecology, Republic of Serbia (Project No. 1470).

APPENDIX

We shall expose the analytical expressions for the quantities a_i, Re d, and f_i, introduced in Sec. III B. For the sake of simplicity, we use the notation α for Re α, b for Re b, etc.

For a_1 and a_3 we have

$$a_1 = \frac{u_0^2}{2\sqrt{2}\beta}, \tag{A1a}$$

$$a_3 = \frac{\beta}{2\sqrt{2}}. \tag{A1b}$$

The quantity a_2 is given by

$$a_2 = \frac{\sqrt{2}}{\beta d}\left(\tilde{\lambda}_\xi d - \frac{\alpha}{16}\lambda_\xi + \epsilon\frac{\beta d}{2\sqrt{2}}(3 - 8du_0^2)\right) - \frac{3}{\sqrt{2}\beta}(3\lambda_\xi^2 + \tau)\frac{\tilde{F}}{b}. \tag{A2}$$

The parameter β figuring in the above expressions, defined by $\beta = \sqrt{h''(u_0)}/2$, can be rewritten in the following form:

$$\beta = 2u_0\left(\frac{1/(4Z-1)}{(1-\alpha u_0^2)^3} - \frac{8Z/(4Z-1)}{(2-\alpha u_0^2)^3} + \frac{\tilde{F}}{2}\right)^{1/2}, \tag{A3}$$

where the quantities u_0 and d are defined in Sec II B. By using these definitions we obtain the following equation for u_0 and d:

$$1 = \frac{2}{\alpha}\left(\frac{1/(4Z-1)}{(1-\alpha u_0^2)^2} - \frac{8Z/(4Z-1)}{(2-\alpha u_0^2)^2}\right) + 2\tilde{F}u_0^2, \tag{A4}$$

$$\frac{1}{4d} = u_0^2 - \frac{2}{\alpha^2}\left(1 + \frac{1/(4Z-1)}{(1-\alpha u_0^2)} - \frac{8Z/(4Z-1)}{(2-\alpha u_0^2)}\right) - \tilde{F}u_0^4. \tag{A5}$$

An approximative expression for the function f_1, defined by Eq. (3.11a), is given by

$$f_1 \approx -\frac{2u_0}{\sqrt{d}}P_0, \tag{A6a}$$

$$P_0 = \frac{1}{2(2+k)}\left(1 + \frac{(1+k)^2}{\sqrt{(2+k)k}}\arcsin\frac{\sqrt{(2+k)k}}{1+k}\right), \tag{A6b}$$

where $k = -2\sqrt{2d}\beta u_0$. The functions f_2 and f_3, defined by Eqs. (3.11b) and (3.11c), can be expressed as

$$f_2 \approx 2(1 - 2\sqrt{2d}\beta u_0) - \ln(2\sqrt{2}\beta u_0^2) + \psi(1/2), \tag{A7a}$$

$$f_3 \approx \frac{3}{2}f_1 + 4u_0\left(\frac{3 - 1/\beta^2}{4\sqrt{d}} - u_0^2\sqrt{d}\right)P_0, \tag{A7b}$$

where $\psi(1/2) \approx -1.963$.

Note that the quantities a_i, $d = \mathrm{Re}\, d$, and f_i represent the known functions of $\mathrm{Re}\,\tilde{E}_\mu$. Indeed, from Eq. (A4) we see that u_0 depends on $\alpha = \alpha(\mathrm{Re}\,\tilde{E}_\mu)$, so that the quantity d from Eq. (A5) is the known function of $\mathrm{Re}\,\tilde{E}_\mu$. Also, the quantity β, given by Eq. (A3), is the $\mathrm{Re}\,\tilde{E}_\mu$-dependent function. Accordingly, from Eqs. (A1a), (A1b), and (A2) we conclude that the quantities a_1, a_2, and a_3 depend on $\mathrm{Re}\,\tilde{E}_\mu$. The same holds for the functions f_1, f_2, and f_3; see Eqs. (A6a) and (A6b), as well as Eqs. (A7a) and (A7b).

[1] S. B. Hill, C. B. Haich, Z. Zhou, P. Nordlander, and F. B. Dunning, Phys. Rev. Lett. **85**, 5444 (2000).
[2] J. Burgdörfer, P. Lerner, and F. Meyer, Phys. Rev. A **44**, 5674 (1991).
[3] J. Burgdörfer, in *Review of Fundamental Processes and Applications of Atoms and Molecules*, edited by C. D. Lin (World Scientific, Singapore, 1997).
[4] U. Wille, Phys. Rev. B **50**, 1888 (1994).
[5] D. Teillet-Billy and J. Gauyacq, Surf. Sci. **239**, 343 (1990).
[6] A. G. Borisov, R. Zimny, D. Teillet-Billy, and J. P. Gauyacq, Phys. Rev. A **53**, 2457 (1996).
[7] P. Nordlander and J. C. Tully, Phys. Rev. Lett. **61**, 990 (1988).
[8] P. Nordlander and J. C. Tully, Phys. Rev. B **42**, 5564 (1990).
[9] P. Nordlander, Phys. Rev. B **53**, 4125 (1996).
[10] V. A. Mandelshtam, T. R. Ravuri, and H. S. Taylor, Phys. Rev. Lett. **70**, 1932 (1993).
[11] J. Muller, X. Yang, and J. Burgdörfer, Phys. Rev. A **49**, 2470 (1994).
[12] P. Kürpick and U. Thumm, Phys. Rev. A **54**, 1487 (1996).
[13] P. Kürpick, U. Thumm, and U. Wille, Phys. Rev. A **57**, 1920 (1998).
[14] N. N. Nedeljković, Lj. D. Nedeljković, S. B. Vojvodić, and M. A. Mirković, Phys. Rev. B **49**, 5621 (1994).
[15] Lj. D. Nedeljković and N. N. Nedeljković, Phys. Rev. B **58**, 16455 (1998).
[16] Lj. D. Nedeljković and N. N. Nedeljković, Phys. Rev. A **67**, 032709 (2003).
[17] N. N. Nedeljković, Lj. D. Nedeljković, and M. A. Mirković, Phys. Rev. A **68**, 012721 (2003).
[18] J. Hanssen, C. F. Martin, and P. Nordlander, Surf. Sci. **423**, L271 (1999).
[19] P. Nordlander and F. B. Dunning, Phys. Rev. B **53**, 8083 (1996).
[20] S. Y. Slavyanov, in *Problems in Mathematical Physics*, edited by M. S. Birman (Leningrad State University, Leningrad, 1970), Vol. 4, p. 125 (in Russian).
[21] S. Y. Slavyanov, Diff. Eq. **5**, 313 (1969) (in Russian).
[22] J. Braun and P. Nordlander, Surf. Sci. **448**, L193 (2000).
[23] V. Kolosov, J. Phys. B **16**, 25 (1983).
[24] R. K. Janev and N. N. Nedeljković, J. Phys. B **19**, 1809 (1985).
[25] Z. Zhou, C. Oubre, S. B. Hill, P. Nordlander, and F. B. Dunning, Nucl. Instrum. Methods Phys. Res. B **193**, 403 (2002).
[26] F. B. Dunning, H. Dunham, C. Oubre, and P. Nordlander, Nucl. Instrum. Methods Phys. Res. B **203**, 69 (2003).